

Article

Numerical Analysis of VPSA Technology Retrofitted to Steam Reforming Hydrogen Plants to Capture CO₂ and Produce Blue H₂

Mauro Luberti ^{1,*}, Alexander Brown ¹ , Marco Balsamo ² and Mauro Capocelli ³ 

¹ Institute for Materials and Processes, School of Engineering, The University of Edinburgh, Robert Stevenson Road, Edinburgh EH9 3FB, UK; alex20_brown@me.com

² Dipartimento di Scienze Chimiche, Università degli Studi di Napoli Federico II, Complesso Universitario di Monte Sant'Angelo, 80126 Napoli, Italy; marco.balsamo@unina.it

³ Research Unit of Process Engineering, Faculty of Engineering, University of Rome "Campus Bio-Medico", Via Alvaro del Portillo 21, 00128 Rome, Italy; m.capocelli@unicampus.it

* Correspondence: mauro.luberti@gmail.com or m.luberti@ed.ac.uk

Abstract: The increasing demand for energy and commodities has led to escalating greenhouse gas emissions, the chief of which is represented by carbon dioxide (CO₂). Blue hydrogen (H₂), a low-carbon hydrogen produced from natural gas with carbon capture technologies applied, has been suggested as a possible alternative to fossil fuels in processes with hard-to-abate emission sources, including refining, chemical, petrochemical and transport sectors. Due to the recent international directives aimed to combat climate change, even existing hydrogen plants should be retrofitted with carbon capture units. To optimize the process economics of such retrofit, it has been proposed to remove CO₂ from the pressure swing adsorption (PSA) tail gas to exploit the relatively high CO₂ concentration. This study aimed to design and numerically investigate a vacuum pressure swing adsorption (VPSA) process capable of capturing CO₂ from the PSA tail gas of an industrial steam methane reforming (SMR)-based hydrogen plant using NaX zeolite adsorbent. The effect of operating conditions, such as purge-to-feed ratio and desorption pressure, were evaluated in relation to CO₂ purity, CO₂ recovery, bed productivity and specific energy consumption. We found that conventional cycle configurations, namely a 2-bed, 4-step Skarstrom cycle and a 2-bed, 6-step modified Skarstrom cycle with pressure equalization, were able to concentrate CO₂ to a purity greater than 95% with a CO₂ recovery of around 77% and 90%, respectively. Therefore, the latter configuration could serve as an efficient process to decarbonize existing hydrogen plants and produce blue H₂.

Keywords: steam methane reforming; CO₂ capture; blue H₂; vacuum pressure swing adsorption; PSA tail gas



Citation: Luberti, M.; Brown, A.; Balsamo, M.; Capocelli, M. Numerical Analysis of VPSA Technology Retrofitted to Steam Reforming Hydrogen Plants to Capture CO₂ and Produce Blue H₂. *Energies* **2022**, *15*, 1091. <https://doi.org/10.3390/en15031091>

Academic Editor: Philippe Leclère

Received: 4 January 2022

Accepted: 28 January 2022

Published: 1 February 2022

Publisher's Note: MDPI stays neutral with regard to jurisdictional claims in published maps and institutional affiliations.



Copyright: © 2022 by the authors. Licensee MDPI, Basel, Switzerland. This article is an open access article distributed under the terms and conditions of the Creative Commons Attribution (CC BY) license (<https://creativecommons.org/licenses/by/4.0/>).

1. Introduction

Because of the constantly rising and unabated greenhouse gas emissions, of which the main constituent is carbon dioxide, the world is experiencing the detrimental effects of climate change. Driven by higher energy and commodity demand, global energy-related CO₂ emissions, led by the power sector, reached a record high of 33.4 Gt in 2019 [1]. To combat climate change, a great deal of research and development has been carried out into low-carbon alternatives to fossil fuels, one of which is represented by hydrogen [2]. As set out in the recently published UK Hydrogen Strategy [3], low-carbon hydrogen will be essential for achieving net zero emissions and meeting a sustainable carbon budget target. Low-carbon hydrogen is particularly useful in decarbonizing sectors with hard-to-abate emission sources, such as the refining, chemical and petrochemical industries, and in providing flexible energy across power, heating and transport sectors. However, despite its great potential, several challenges need to be solved before hydrogen can be adopted as

a common low-carbon energy carrier such as a well-planned synergy among production, transmission, storage and distribution.

The global demand for hydrogen in its pure form is currently around 72 million tonnes per year, with the ammonia and refining industries consuming over 90% of the production capacity [2]. The methanol and steel industries consume an additional 16 million tonnes per year of hydrogen as a mixture of gases [2]. The production of hydrogen is carried out using around 90% of feedstock as fossil fuels, including natural gas as the largest share, fuel oil and coal [2]. At present, steam methane reforming (SMR) is the most widespread process to produce hydrogen from natural gas and light hydrocarbons. The majority of SMR-based hydrogen plants are fully optimized in order to achieve CO₂ emissions close to the theoretical minimum [4]. However, the further reduction of 830 million tonnes of CO₂ emitted from hydrogen plants worldwide [2] could only be obtained by integrating carbon capture and storage (CCS) technologies in the hydrogen plant, thus allowing the production of low-carbon hydrogen known as blue H₂.

The block flow diagram for a typical SMR-based hydrogen plant is shown in Figure 1. From the battery limits, the natural gas feed is purified, pre-reformed and reformed to produce a syngas stream. The process is generally followed by a single stage of high temperature water gas shift (WGS) reactor, since a very low CO residual is not required. Any CO remaining in the raw hydrogen is recovered as reformer fuel. After cooling, the shifted syngas is purified in a pressure swing adsorption (PSA) unit to achieve ultrapure H₂ (99.99+%). Depending on the operating conditions, the typical PSA tail gas comprises 45–55 mol% CO₂, 20–25 mol% H₂, 10–15 mol% CH₄, 10–15 mol% CO and 1–5 mol% N₂ [4]. Given its high lower heating value, the PSA tail gas is sent back to the reformer burners along with a fraction of the natural gas feed as a fuel. From the block flow diagram of Figure 1, three distinct CO₂ capture locations can be identified: the shifted syngas (location 1) having the highest CO₂ partial pressure, the PSA tail gas (location 2) having the highest CO₂ concentration and the flue gas (location 3) having the highest CO₂ flowrate. The three capture locations have been extensively assessed in the literature [5–7].

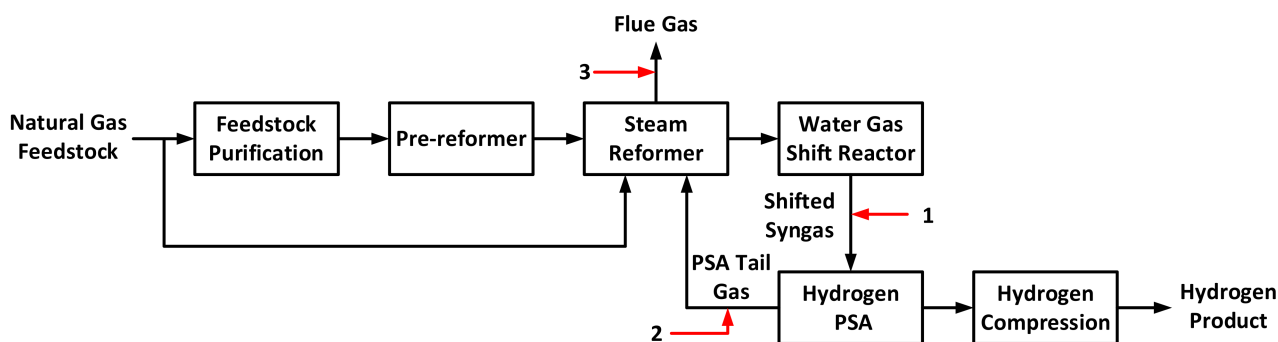


Figure 1. Block flow diagram for the SMR process. Carbon capture technologies can be applied at the locations marked with a red arrow.

To date, several pilot plants have demonstrated the viability of low-carbon hydrogen production using the SMR process coupled with CCS based on chemical absorption, adsorption, membranes and cryogenic distillation. The Shell Quest Project in Canada demonstrated the feasibility of aqueous amine solutions-based absorption technology, with the capacity to capture approximately 1.1 million tonnes of CO₂ per annum (Mtpa) [8]. The Port Arthur Project in USA used vacuum swing adsorption technology having a CO₂ capture capacity of around 1.0 Mtpa [9]. In France, the Port Jerome Project demonstrated the viability of cryogenic and membrane separation through the Air Liquide CryocapTM system, resulting in a CO₂ capture capacity of around 0.1 Mtpa [10].

Among the proposed carbon capture technologies, adsorption processes have proven to be less energy intensive [11–13] with higher operating flexibility and lower maintenance costs when compared to other purification pathways [4,14,15]. In the SMR-based hydrogen

plant, only the flue gas capture location has the potential to fully decarbonize the plant by removing all the CO₂ emissions but is characterized by the lowest CO₂ partial pressure and concentration, thus requiring several large vacuum pressure swing adsorption (VPSA) units to operate in parallel. To partly alleviate the resulting high CAPEX and OPEX, the use of rapid cycles has been proposed in the literature [13,16]. The shifted syngas capture location features the highest CO₂ partial pressure. However, it is well known that, in order to obtain a high-purity CO₂ product, PSA cycles must be operated under vacuum desorption pressure to fully regenerate the adsorption beds packed with zeolitic adsorbents, thus incurring large pressure swing energy penalties [17,18]. In addition, depending on the pressure drops, the CO₂-depleted syngas stream may need to be recompressed prior to the H₂ PSA unit and/or the H₂ PSA unit may have to be reconfigured to take into account the substantial change in feed flowrate and composition. For instance, Liu et al. [18] demonstrated that, with very similar CO₂ purities and recoveries, a CO₂ VPSA process first followed by a H₂ PSA process underperformed a H₂ PSA process first followed by a CO₂ VPSA process since the specific energy consumption was around 14% higher while the H₂ recovery was around 16% lower. To overcome these economic limitations, some authors have investigated the integration of hydrogen purification and CO₂ capture in a single adsorption cycle [19–21]. However, this novel adsorption process would be suitable only for greenfield hydrogen plants potentially equipped with a second-stage low temperature WGS reactor, leading to a higher CO conversion prior to the integrated VPSA unit. Therefore, the PSA tail gas, having the highest CO₂ concentration, is expected to be the most economically efficient carbon capture location to retrofit existing hydrogen plants via VPSA technology.

In the literature, only a few studies have been carried out tackling this kind of separation. Golmakani et al. [22] designed and simulated a 4-bed, 7-step VPSA process comparing three adsorbents, namely activated carbon, 5A zeolite and SAPO-34 zeolite, and assessing the effect of several operating conditions such as weight-hourly space velocity, feed pressure, vacuum pressure and purge-to-feed ratio on the process performances. After a detailed sensitivity analysis, it was concluded that the VPSA process using SAPO-34 could enrich CO₂ to purity levels greater than 90% with a recovery of around 73%. Shi et al. [23] investigated the performance of a 3-bed, 5-step VPSA process using silica gel as an adsorbent. They found that the adsorption pressure exhibited the highest influence on both CO₂ purity and specific energy consumption, while the bed diameter was the dominant parameter in regulating the CO₂ recovery. The best simulation runs achieved a CO₂ purity of 97.1% with a recovery of 82.6%, or a CO₂ purity of 88.6% with a recovery of 97.8%.

It should be noted that both the abovementioned scientific works considered a lab-scale feed flowrate for the VPSA process, which is 3–5 orders of magnitude lower than that of industrial hydrogen plants. Industrial fixed-bed adsorbents are characterized by higher superficial velocities, higher pressure drops, higher mass and heat transfer coefficients, and quasi-adiabatic operation, all of which will affect the separation performance [13,24]. Moreover, in both cited papers the CO concentration in the VPSA feed was in the range of only 1.0–1.5 mol%, assuming a two-stage WGS reaction (in contrast with 10–15 mol% of a single stage) that is unconventional in hydrogen plants. Accordingly, the separation performance of the VPSA process would be overestimated since for most adsorbents the selectivity of CO₂ over CO is the lowest compared to the other feed components (CH₄, N₂, H₂).

Therefore, in this study we overcame for the first time the above limitations by designing and numerically investigating a VPSA process capable of capturing CO₂ from the PSA tail gas of an industrial SMR-based hydrogen plant equipped with a conventional single stage high temperature WGS reactor. The separation performance targets were 95+% CO₂ purity and 90+% CO₂ recovery. To this end, conventional cycle configurations, namely 2-bed, 4-step Skarstrom cycle (composed of adsorption, blowdown, purge and feed pressurization steps) and 2-bed, 6-step modified Skarstrom cycle with pressure equalization, were assessed by means of a rigorous mathematical model accounting for mass, energy and momentum balance equations along with various operating parameters such as the

purge-to-feed ratio and the desorption pressure. The selected adsorbent was NaX zeolite from Union Carbide, which has been recently tested by Brea et al. [25] in PSA cycles for hydrogen purification. NaX zeolite also exhibits excellent adsorption properties for CO₂ capture in terms of saturation capacity, working capacity and CO₂ selectivity over the other components in the PSA tail gas, as extensively reported in the literature [11–13,26,27].

2. VPSA Mathematical Model

To accurately simulate a VPSA system, a rigorous mathematical model was used to integrate mass, momentum and energy balances along an adsorption packed bed [28,29].

Since the gas flow was assumed as an axially dispersed plug flow, Equation (1) gives the component mass balance:

$$\frac{\partial c_i}{\partial t} + \frac{\partial J_i}{\partial z} + \frac{\partial(u \cdot c_i)}{\partial z} + \frac{1 - \varepsilon}{\varepsilon} \cdot \rho_s \cdot \frac{\partial \bar{q}_i}{\partial t} = 0 \quad (1)$$

where

$$J_i = -D_z \cdot c_T \cdot \frac{\partial y_i}{\partial z} \quad (2)$$

To estimate the gas velocity along the bed the following overall mass balance needs to be solved:

$$\frac{\partial c_T}{\partial t} + \frac{\partial(u \cdot c_T)}{\partial z} + \frac{1 - \varepsilon}{\varepsilon} \cdot \rho_s \cdot \sum_{i=1}^n \frac{\partial \bar{q}_i}{\partial t} = 0 \quad (3)$$

Since the bed undergoes significant variations in temperature due to the heats of adsorption, the energy balance is expressed as:

$$\frac{\partial U_g}{\partial t} + \frac{1 - \varepsilon}{\varepsilon} \cdot \frac{\partial U_s}{\partial t} + \frac{\partial J_T}{\partial z} + \frac{\partial(u \cdot H_g)}{\partial z} - \frac{1 - \varepsilon}{\varepsilon} \cdot \rho_s \cdot \sum_{i=1}^n (-\Delta \bar{H}_i) \cdot \frac{\partial \bar{q}_i}{\partial t} + \frac{4 \cdot h_w}{D_b} (T - T_w) = 0 \quad (4)$$

where

$$J_T = -k_z \cdot \frac{\partial T}{\partial z} \quad (5)$$

In this study, the effect of kinetic energy in the energy balance was neglected as the VPSA cycles were not rapid [30]. In addition, the bed wall temperature was assumed to be 301.15 K.

The momentum balance was described by the Ergun equation [31], for which the pressure drop along the bed can be evaluated as follows:

$$-\frac{dP}{dz} = \frac{150 \cdot \mu \cdot (1 - \varepsilon)^2 \cdot u}{d_p^2 \cdot \varepsilon^2} + \frac{1.75 \cdot (1 - \varepsilon) \cdot \rho_g \cdot u \cdot |u|}{d_p \cdot \varepsilon} \quad (6)$$

The Danckwerts boundary conditions were taken for the gas phase concentrations and the enthalpies. Considering as a positive the flow direction from 0 (feed end) to L (product end), they can be expressed in general terms as:

$$J_i|_{z=0} = \frac{u + |u|}{2} \cdot (c_{i,0-} - c_{i,0}) \quad (7)$$

$$J_i|_{z=L_b} = \frac{u - |u|}{2} \cdot (c_{i,L_b+} - c_{i,L_b}) \quad (8)$$

$$J_T|_{z=0} = \frac{u + |u|}{2} \cdot (H_{g,0-} - H_{g,0}) \quad (9)$$

$$J_T|_{z=L_b} = \frac{u - |u|}{2} \cdot (H_{g,L_b+} - H_{g,L_b}) \quad (10)$$

Experimental adsorption equilibrium of H₂, CH₄, CO and CO₂ on NaX zeolite were reported by Brea et al. [25] at three temperatures (298, 313 and 338 K) and in the pressure

range of 0–3 bar, which is sufficient to characterize the operating pressure ranges of the analyzed VPSA systems. The ideal adsorbed solution theory (IAST) was used to predict multicomponent adsorption equilibria. The resulting system of algebraic-integral equations that needs to be solved is as follows [32,33]:

$$P \cdot y_i = P_i^0 \cdot x_i \quad (11)$$

$$\psi_i = \int_0^{P_i^0} q_i \cdot d(\ln P_i) \quad (12)$$

$$\psi_i = \psi_{eq} \quad (13)$$

$$\frac{1}{q_T} = \sum_{i=1}^n \left(\frac{x_i}{q_i} \right) \quad (14)$$

Following the fitting reported by Brea et al. [25], the dual-site Langmuir model was used to describe the pure component adsorption isotherms:

$$q_i^* = \frac{q_{s1,i} \cdot b_{1,i} \cdot P_i}{1 + b_{1,i} \cdot P_i} + \frac{q_{s2,i} \cdot b_{2,i} \cdot P_i}{1 + b_{2,i} \cdot P_i} \quad (15)$$

where

$$b_{n,i} = b_{n,i,0} \exp\left(\frac{-\Delta H_{n,i}}{R \cdot T}\right) \quad n = 1, 2 \quad (16)$$

The dual-site Langmuir isotherm parameters were attained by regressing the experimental data in the operating condition ranges using Origin software [34]. Given the heterogeneity of the isotherm model, the heat of adsorption in the energy balance (Equation(4)) was averaged on the two adsorption sites.

Mass transfer in the adsorbent particle was described by the Linear Driving Force (LDF) model following the approach by Brea et al. [25]:

$$\frac{\partial \bar{q}_i}{\partial t} = k_{LDF,i} \cdot (q_i^* - \bar{q}_i) \quad (17)$$

where

$$k_{LDF,i} = k_{1,i} \cdot T + k_{2,i} \quad (18)$$

From the experimental data, the reciprocal time constants, and hence the LDF coefficients, were linearly regressed in the reported temperature range for CH₄, CO and CO₂ while H₂ LDF coefficient was set to a very high value to represent that H₂ does not exhibit diffusional limitations during adsorption [25]. All equilibrium and kinetic parameters of this study for NaX zeolite can be found in Table 1.

Table 1. Equilibrium and kinetic parameters for NaX zeolite. Data were regressed from [25].

Equilibrium Parameter (Dual-Site Langmuir Isotherm)	q_{s1}/q_{s2} (mol kg ⁻¹)	b_{01}/b_{02} (bar ⁻¹)	$(-\Delta H_1)/(-\Delta H_2)$ (J mol ⁻¹)
H ₂	4.529/0	$2.431 \times 10^{-4}/0$	7018/0
CH ₄	4.529/0	$8.313 \times 10^{-5}/0$	16,294/0
CO	4.529/0	$9.411 \times 10^{-5}/0$	18,182/0
CO ₂	2.500/2.029	$3.521 \times 10^{-5}/6.318 \times 10^{-6}$	32,244/30,937
Kinetic Parameter ($k_{LDF} = k_1 \times T + k_2$)	k_1 (s ⁻¹ K ⁻¹)	k_2 (s ⁻¹)	
H ₂	0	100	
CH ₄	0.0115	-2.8561	
CO	0.0137	-3.6086	
CO ₂	0.0099	-2.8631	

The correlations proposed by Wakao and Funazkri [35] were used to estimate the axial mass dispersion coefficient D_z and the axial thermal dispersion coefficient k_z :

$$\frac{\varepsilon \cdot D_z}{D_m} = 20 + 0.5 \cdot Sc \cdot Re \quad (19)$$

$$\frac{k_z}{k_g} = 7 + 0.5 \cdot Pr \cdot Re \quad (20)$$

The correlation by Specchia et al. [36] was used to calculate the internal heat transfer coefficient between the gas and the bed wall:

$$h_w = \frac{k_g}{d_p} \cdot (0.0835 \cdot Re^{0.91}) \quad (21)$$

Eventually, Multiflash coupled with the ideal gas law [37] was used to evaluate the remaining gas mixture physical properties such as density, thermal conductivity, viscosity and molar specific heat.

To complete the mathematical model of a VPSA system, the adsorption beds have to be integrated in a realistic flowsheet by means of ancillary equipment, including valves, headers, sources and sinks [38]. In particular, two valve models were considered, either mass flow controller (MFC) or pressure-driven mode (PDM):

$$F = F_i \text{ (MFC)} \quad (22)$$

$$F = V_{SP} \cdot C_v \cdot \sqrt{\Delta P} \text{ (PDM)} \quad (23)$$

Full details of the mathematical model of ancillary units can be found elsewhere [29].

In a carbon capture application by VPSA technology CO_2 is usually the most strongly adsorbent component so that it is recovered during the blowdown step and the purge step. Thus, the key performance indicators (KPIs) for this separation are the following:

$$\text{CO}_2 \text{ Purity} = \frac{\int_0^{t_{BD}} c_{\text{CO}_2} \cdot u|_{z=0} dt + \int_0^{t_{PU}} c_{\text{CO}_2} \cdot u|_{z=0} dt}{\sum_{i=1}^n \int_0^{t_{BD}} c_i \cdot u|_{z=0} dt + \sum_{i=1}^n \int_0^{t_{PU}} c_i \cdot u|_{z=0} dt} \quad (24)$$

$$\text{CO}_2 \text{ Recovery} = \frac{\int_0^{t_{BD}} c_{\text{CO}_2} \cdot u|_{z=0} dt + \int_0^{t_{PU}} c_{\text{CO}_2} \cdot u|_{z=0} dt}{\int_0^{t_{AD}} c_{\text{CO}_2} \cdot u|_{z=0} dt + \int_0^{t_{PR}} c_{\text{CO}_2} \cdot u|_{z=0} dt} \quad (25)$$

$$\text{Bed Productivity} = \frac{\left(\int_0^{t_{BD}} c_{\text{CO}_2} \cdot u|_{z=0} dt + \int_0^{t_{PU}} c_{\text{CO}_2} \cdot u|_{z=0} dt \right) \cdot A_b}{t_{\text{cycle}} \cdot m_{\text{ads}}} \quad (26)$$

$$\text{Specific Energy} = \frac{\int_0^{t_{BD}+t_{PU}} \text{Power}_{\text{vacuum}} dt}{\left(\int_0^{t_{BD}} c_{\text{CO}_2} \cdot u|_{z=0} dt + \int_0^{t_{PU}} c_{\text{CO}_2} \cdot u|_{z=0} dt \right) \cdot MW_{\text{CO}_2} \cdot A_b} \quad (27)$$

$$\text{Power}_{\text{vacuum}} = \frac{1}{\eta} \cdot F \cdot \frac{\gamma}{\gamma - 1} \cdot \left(\frac{P_{\text{des}}}{\rho_g} \right) \cdot \left[\left(\frac{P_{\text{atm}}}{P_{\text{des}}} \right)^{\frac{\gamma-1}{\gamma}} - 1 \right] \quad (28)$$

where Equations (27) and (28) were used to calculate the specific energy required for the process. This was obtained as the ratio of the power consumption of the vacuum pump and the mass flowrate of CO_2 at the cyclic steady state (CSS). For all the VPSA configurations of this study, the cyclic steady state was reached after 50–60 cycles when the difference of CO_2 purity and recovery with respect to the previous cycle were both less than 10^{-5} .

The VPSA mathematical model was solved using gProms software [37]. Second order centered finite difference method (CFDM) with 100 elements along the bed length

was chosen as discretization method. Both absolute and relative numerical tolerances were set to 10^{-6} .

3. Design Basis and Cycle Configurations

This study was based on the SMR plant outlined in the technical report by the International Energy Agency Greenhouse Gas R&D Programme [39]. The report provides a techno-economic assessment of an industrial SMR-based hydrogen plant without and with CCS having a nominal capacity of $100,000 \text{ Nm}^3 \text{ h}^{-1}$ of H_2 and operating as a standalone plant. The base case plant without CCS comprises a feedstock pre-treatment, a pre-reformer, a primary reformer, a high temperature WGS reactor, a H_2 PSA in single train arrangement and a multi-stage hydrogen compression. The plant consumes around $14.2 \text{ MJ}_{\text{th}}$ of natural gas, emits around 0.81 kg of CO_2 per Nm^3 of H_2 produced and has a surplus of around 9.9 MW_e electricity exported to the grid. The PSA tail gas, regarded as the feed stream of the CO_2 VPSA unit, is extracted at 1.3 bar and 301.15 K and has a molar composition of $23.69\% \text{ H}_2$, $0.62\% \text{ N}_2$, $9.45\% \text{ CH}_4$, $14.54\% \text{ CO}$, $50.95\% \text{ CO}_2$ and $0.76\% \text{ H}_2\text{O}$. The associated flowrate is $60,658 \text{ kg h}^{-1}$ that corresponds to 585.1 mol s^{-1} . The detailed process flow diagram of the plant along with full material and energy balances can be found in the IEA report [39].

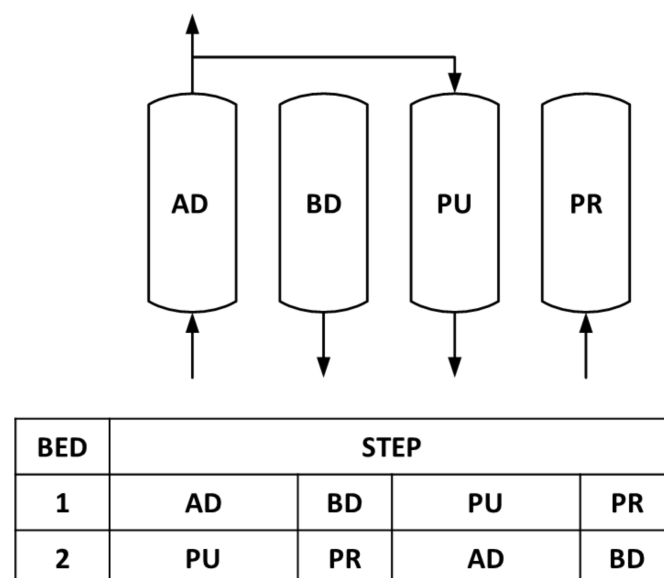
For simplicity, the PSA tail gas was assumed to be dehydrated in a pre-treatment drying process where the water amount was reduced down to ppm levels. Due to the unavailability of nitrogen isotherms on NaX adsorbent [25], nitrogen was lumped into methane, which makes the simulations conservative in terms of CO_2 capture as methane is more strongly adsorbed than nitrogen in zeolites [14,40]. Therefore, the resulting VPSA feed molar composition was $23.87\% \text{ H}_2$, $10.15\% \text{ CH}_4$, $14.65\% \text{ CO}$ and $51.34\% \text{ CO}_2$. Physical properties of NaX zeolite were taken from Brea et al. [25], however a typical industrial pellet diameter of 2.5 mm was considered from the literature. We also assumed that the specific heat capacity of the adsorbent was $920 \text{ J kg}^{-1} \text{ K}^{-1}$, similar to other 13X zeolite pellets [13].

Industrial VPSA beds exhibit superficial velocities in the range $0.1\text{--}0.5 \text{ m s}^{-1}$ and are designed with diameters up to 3.0 m in order to minimize pressure drops while ensuring even distribution of the gas flow along the bed [24]. Given the very large volumetric flowrate of the PSA tail gas, four VPSA trains with a bed diameter of 3.0 m were designed to operate in parallel. The resulting volumetric feed flowrate per PSA train was $2.82 \text{ m}^3 \text{ s}^{-1}$ corresponding to a molar flowrate of $146.27 \text{ mol s}^{-1}$ while the superficial velocity was approximately 0.4 m s^{-1} . The L_b/D_b ratio was selected in the range $1.5\text{--}2.0$ in order to have a cycle time of around 10 min along with bed pressure drops less than 0.1 bar . A full list of adsorbent parameters, bed parameters and operating conditions for the VPSA process is reported in Table 2.

In this study, a first 2-bed, 4-step Skarstrom cycle with vacuum desorption pressure was assessed, as depicted in Figure 2. After the adsorption step, the first bed is depressurized to the desorption pressure during the blowdown step. At the same time, the feed mixture is switched to the second bed to repressurize it, followed by the adsorption step at the feed pressure. A fraction of the raffinate effluent from the second bed is passed through the first bed, countercurrently, to purge the bed at the desorption pressure. This minimizes the amount of residual carbon dioxide in the bed, returning it to a clean state. After the purge, the VPSA unit is ready for the next cycle so that each bed undergoes two half-cycles, the times of which are equal [14,40].

Table 2. Adsorbent parameters, bed parameters, valve parameters and operating conditions for the VPSA process.

Adsorbent Parameters	
ρ_s (kg m ⁻³)	1256 [25]
ε_p (-)	0.404 [25]
$c_{p,s}$ (J kg ⁻¹ K ⁻¹)	920 [13]
d_p (m)	2.5×10^{-3} [13]
Bed Parameters	
L_b (m)	4.5 (2-bed, 4-step); 6.0 (2-bed, 6-step)
D_b (m)	3.0
ε (-)	0.53 [25]
D_z (m ² s ⁻¹)	1.5×10^{-3}
k_z (W m ⁻¹ K ⁻¹)	1.4
h_w (W m ⁻² K ⁻¹)	55.1
Valve Parameters	
C_v (kg s ⁻¹ Pa ^{-1/2})	1.0×10^{-3} (feed)
	1.0×10^{-3} (product)
	5.0×10^{-3} (blowdown)
	1.5×10^{-3} (purge top)
	5.0×10^{-3} (purge bottom)
	3.0×10^{-4} (equalization)
Operating Conditions	
Feed composition (mol%)	23.87% H ₂ ; 10.15% CH ₄ ; 14.65% CO; 51.34% CO ₂
Adsorption pressure (bar)	1.3
Desorption pressure (bar)	0.05–0.2
Purge-to-feed ratio (-)	0–0.05
Feed temperature (K)	301.15
Molar feed flowrate (mol s ⁻¹)	146.27 (per PSA train)
Volumetric feed flowrate (m ³ s ⁻¹)	2.82 (per PSA train)

**Figure 2.** Configuration of the 2-bed, 4-step Skarstrom cycle (AD: Adsorption, BD: Blowdown, PU: Purge, PR: Feed pressurization; $t_{AD} = t_{PU} = 250$ s, $t_{BD} = t_{PR} = 50$ s).

In a vacuum swing cycle using the same adsorption pressure of a cycle having an atmospheric desorption pressure, for the same CO₂ purity, the CO₂ recovery is increased at the expense of additional energy required to run the vacuum pump. To partly compensate

the increase in energy consumption, a second 2-bed, 6-step modified Skarstrom cycle with pressure equalization and vacuum desorption pressure was considered, which is shown in Figure 3. After the first bed has finalized the adsorption step and the second bed has been purged, the two beds are connected in order to equalize their pressure. This step conserves energy because the compressed gas from a high-pressure bed is used to partially pressurize a low-pressure bed. As a result, the CO₂ purity can be improved with the same CO₂ recovery [14,40].

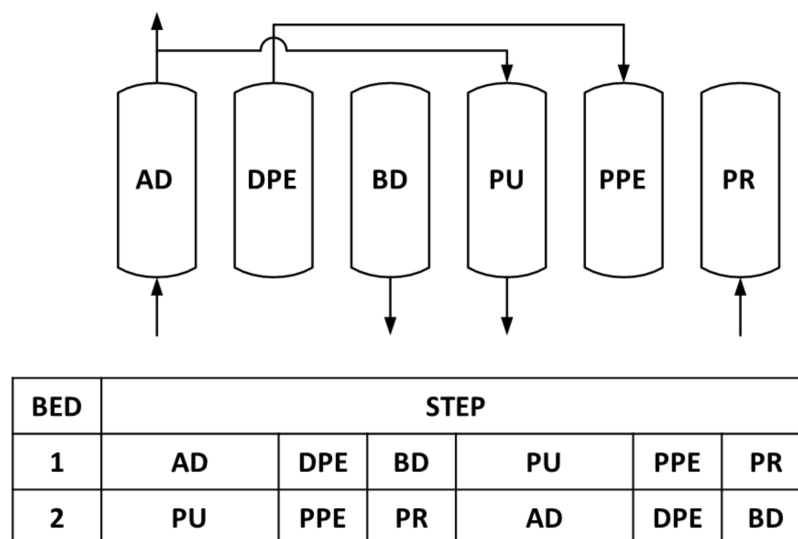


Figure 3. Configuration of the 2-bed, 6-step modified Skarstrom cycle with pressure equalization (AD: Adsorption, DPE: Depressurizing pressure equalization, BD: Blowdown, PU: Purge, PPE: Pressurizing pressure equalization, PR: Feed pressurization; $t_{AD} = t_{PU} = 250$ s, $t_{BD} = t_{PR} = 50$ s, $t_{DPE} = t_{PPE} = 25$ s).

For the 2-bed, 4-step configuration the total cycle time was fixed at 600 s with $t_{AD} = t_{PU} = 250$ s and $t_{BD} = t_{PR} = 50$ s (Figure 2). The adsorption/purge step time was set sufficiently below the CO₂ breakthrough time observed in breakthrough simulations while the blowdown/pressurization step time was set to allow sufficient time for the pressure change. The 2-bed, 6-step cycle time was fixed at 650 s with $t_{AD} = t_{PU} = 250$ s, $t_{BD} = t_{PR} = 50$ s and $t_{DPE} = t_{PPE} = 25$ s (Figure 3). At the beginning of each simulation, the beds were assumed to be filled with pure hydrogen at the adsorption or desorption pressure depending on the cycle step and at 301.15 K. The valve flow coefficients were correctly calibrated in function of the cycle step(s) in which the valves were open, with the values reported in Table 2.

4. Results and Discussion

Once the industrial fixed-bed adsorbers were sized and the cycle step times selected, the separation KPIs were assessed for both configurations by varying operating conditions such as the purge-to-feed ratio (P/F ratio) and the vacuum desorption pressure. These operating parameters have been extensively evaluated in the literature for CO₂ capture processes by VPSA technology [11–13,22]. In particular, the power consumption of the VPSA unit would be highly dependent on the selected desorption pressure as long as the P/F ratio was low enough to achieve high CO₂ product purities. To meet the separation targets of this study, i.e., 95+% CO₂ purity and 90+% CO₂ recovery, the investigated desorption pressure was in the range 0.05–0.2 bar while the P/F ratio was varied between 0 and 0.05 (Table 2). Given the industrial feed flowrate and the relatively low vacuum desorption pressures, the vacuum pump was assumed a liquid-ring pump and its efficiency (η) was evaluated at 40%, in line with VPSA experimental and modelling studies reported in the literature [27,29].

4.1. 2-Bed, 4-Step Simulations

For the 2-bed, 4-step VPSA configuration, 12 simulation runs were carried out until a cyclic steady state was achieved. All performance results are summarized in Table 3 in terms of CO₂ purity, CO₂ recovery, specific energy consumption and bed productivity. The unit KPIs are also shown in Figure 4 in terms of P/F ratio with variable desorption pressure. As expected, higher P/F ratios increase the CO₂ recovery (Figure 4b) because the adsorption beds will be regenerated to a higher extent, thus reducing the CO₂ loss during the subsequent adsorption step. On the contrary, the CO₂ purity is decreased (Figure 4a) as more purge light gases will be extracted along with the CO₂ in the purge vent. The bed productivity also increases with the P/F ratio following the CO₂ recovery trend (Figure 4d). Even if CO₂ recovery raises with the P/F ratio, the CO₂ purity reduces, resulting in an increase of the purge light gases recovery, which ultimately leads to a moderate increase of the specific power consumption (Figure 4c). For instance, at the desorption pressure of 0.05 bar the specific energy consumption is 691.3 kJ kg_{CO₂}⁻¹ with P/F = 0.05, a value that is 6.5% greater than the outcome obtained with P/F = 0. As anticipated, the effect of desorption pressure is more significant on the KPIs. Shifting the desorption pressure from 0.2 to 0.05 bar, CO₂ purities and recoveries are improved by 3–5% and 30–40%, respectively, at the expense of the specific energy consumption that approximately doubled (Figure 4).

Table 3. Performance results of the 2-bed, 4-step VPSA process.

Run #	P _{des} (bar)	P/F Ratio (–)	CO ₂ Purity (%)	CO ₂ Recovery (%)	Specific Energy Consumption (kJ kg _{CO₂} ⁻¹)	Bed Productivity (mol _{CO₂} h ⁻¹ kg _{ads} ⁻¹)
Run 1	0.05	0	95.3	77.4	649.1	5.57
Run 2		0.01	94.5	80.7	654.7	5.81
Run 3		0.03	92.1	85.0	671.7	6.12
Run 4		0.05	89.7	88.0	691.3	6.33
Run 5	0.1	0	93.8	60.1	475.2	4.33
Run 6		0.01	93.4	66.5	477.0	4.79
Run 7		0.03	91.3	72.8	488.7	5.24
Run 8		0.05	89.0	77.0	501.7	5.54
Run 9	0.2	0	89.9	37.5	327.3	2.70
Run 10		0.01	90.2	45.9	324.1	3.30
Run 11		0.03	89.1	53.7	330.1	3.86
Run 12		0.05	87.0	58.8	338.1	4.23

Run 1 in Table 3, having a desorption pressure of 0.05 bar and a P/F ratio equal to 0, achieved the best CO₂ capture targets, i.e., CO₂ purity of 95.3% and CO₂ recovery of 77.4% with a bed productivity of 5.57 mol_{CO₂} h⁻¹ kg_{ads}⁻¹ and a specific energy consumption of 649.1 kJ kg_{CO₂}⁻¹. However, the CO₂ recovery rate was deemed too low to effectively decarbonize existing hydrogen plants, so a more complex VPSA configuration incorporating a pressure equalization step was investigated.

4.2. 2-Bed, 6-Step Simulations

Given the unsatisfactory performance results of the 2-bed, 4-step configuration, 12 additional simulation runs were carried out assessing the 2-bed, 6-step configuration, with performance results reported in Table 4 and graphically displayed in Figure 5. Generally, the KPIs exhibited the same trends as the previous cycle configuration but it should be noted that, with a CO₂ purity above 96%, the CO₂ recovery reached a value close to 90% in Run 15. The enhanced CO₂ recovery of about 13% points with respect to the previously analysed configuration came as the result of incorporating the pressure equalization step in the cycle. The specific energy consumption (639.7 kJ kg_{CO₂}⁻¹) was very similar to that of the previous cycle configuration while the bed productivity was decreased from 5.57 to 4.47 mol_{CO₂} h⁻¹ kg_{ads}⁻¹, which was mainly due to the increased adsorption bed length. In summary, it is expected that a 2-bed, 6-step VPSA system with a desorption pressure of 0.05 bar and a P/F ratio slightly higher than 0.03 would be able

to successfully meet the required capture targets of CO₂ purity and CO₂ recovery greater than 95% and 90%, respectively.

Table 4. Performance results of the 2-bed, 4-step VPSA process.

Run #	P _{des} (bar)	P/F Ratio (-)	CO ₂ Purity (%)	CO ₂ Recovery (%)	Specific Energy Consumption (kJ kg _{CO₂} ⁻¹)	Bed Productivity (mol _{CO₂} h ⁻¹ kg _{ads} ⁻¹)
Run 13	0.05	0	99.1	84.2	621.5	4.20
Run 14		0.01	98.5	86.1	625.4	4.29
Run 15		0.03	96.4	89.7	639.7	4.47
Run 16		0.05	94.1	92.4	657.8	4.60
Run 17	0.1	0	98.5	69.1	450.9	3.44
Run 18		0.01	97.9	73.2	453.5	3.65
Run 19		0.03	95.8	79.0	463.9	3.94
Run 20		0.05	93.6	83.1	476.4	4.14
Run 21	0.2	0	96.1	45.3	305.1	2.26
Run 22		0.01	95.9	51.1	305.7	2.55
Run 23		0.03	94.1	59.3	311.9	2.95
Run 24		0.05	91.9	64.8	319.9	3.23

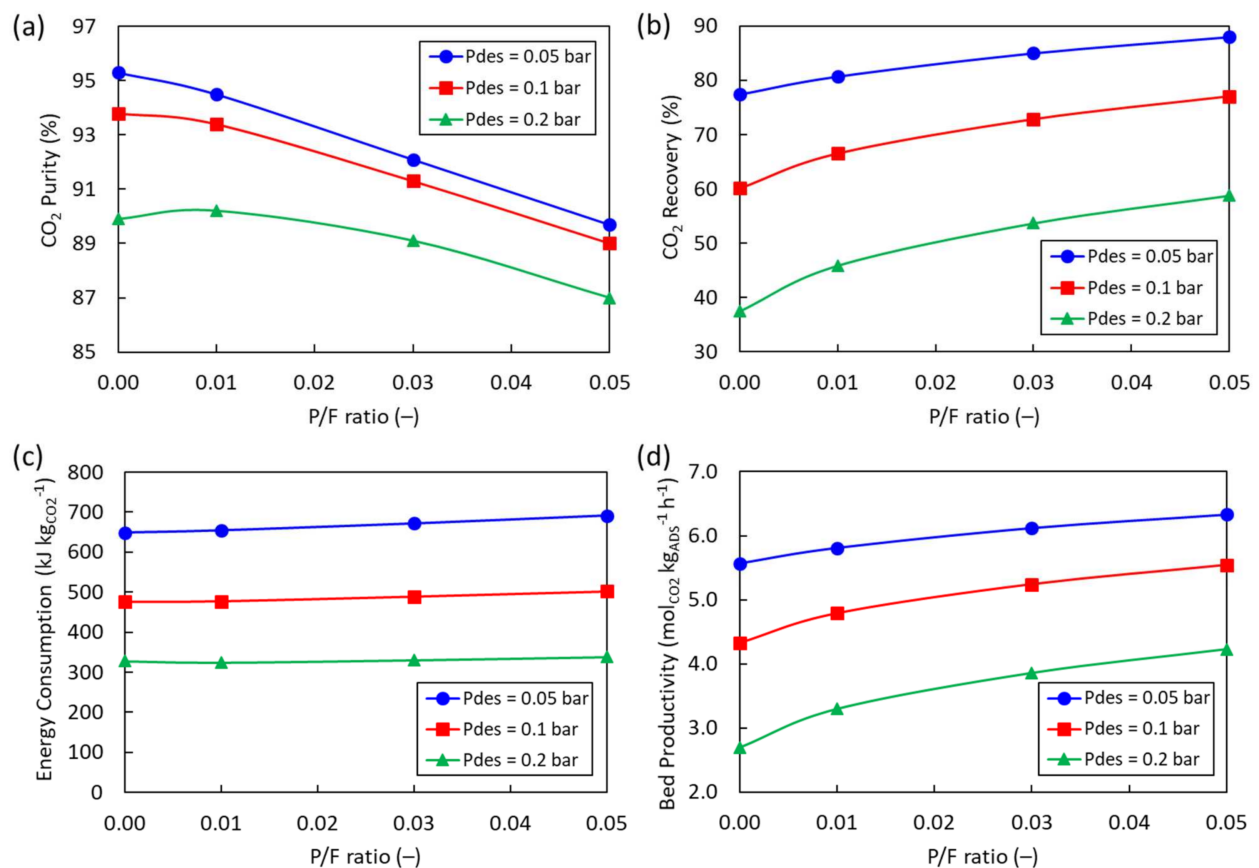


Figure 4. Evolution of the KPIs of the 2-bed, 4-step VPSA with the purge-to-feed ratio and desorption pressure: (a) CO₂ purity; (b) CO₂ recovery; (c) Specific energy consumption; (d) Bed productivity.

4.3. Cycle Configuration Comparison

Runs 6 and 18 are compared in terms of pressure and temperature profiles averaged over the bed length for a cycle in Figures 6 and 7, respectively. Both runs have a desorption pressure of 0.1 bar and a P/F ratio of 0.01. In the 2-bed, 6-step configuration (Run 18) the pressure equalizes in the bed at around 0.5 bar (Figure 7a). The largest temperature swing in a cycle is in the range 30–35 °C for both configurations, which is expected given the high CO₂ content in the feed and the partial CO₂ breakthrough in the bed at cyclic steady state.

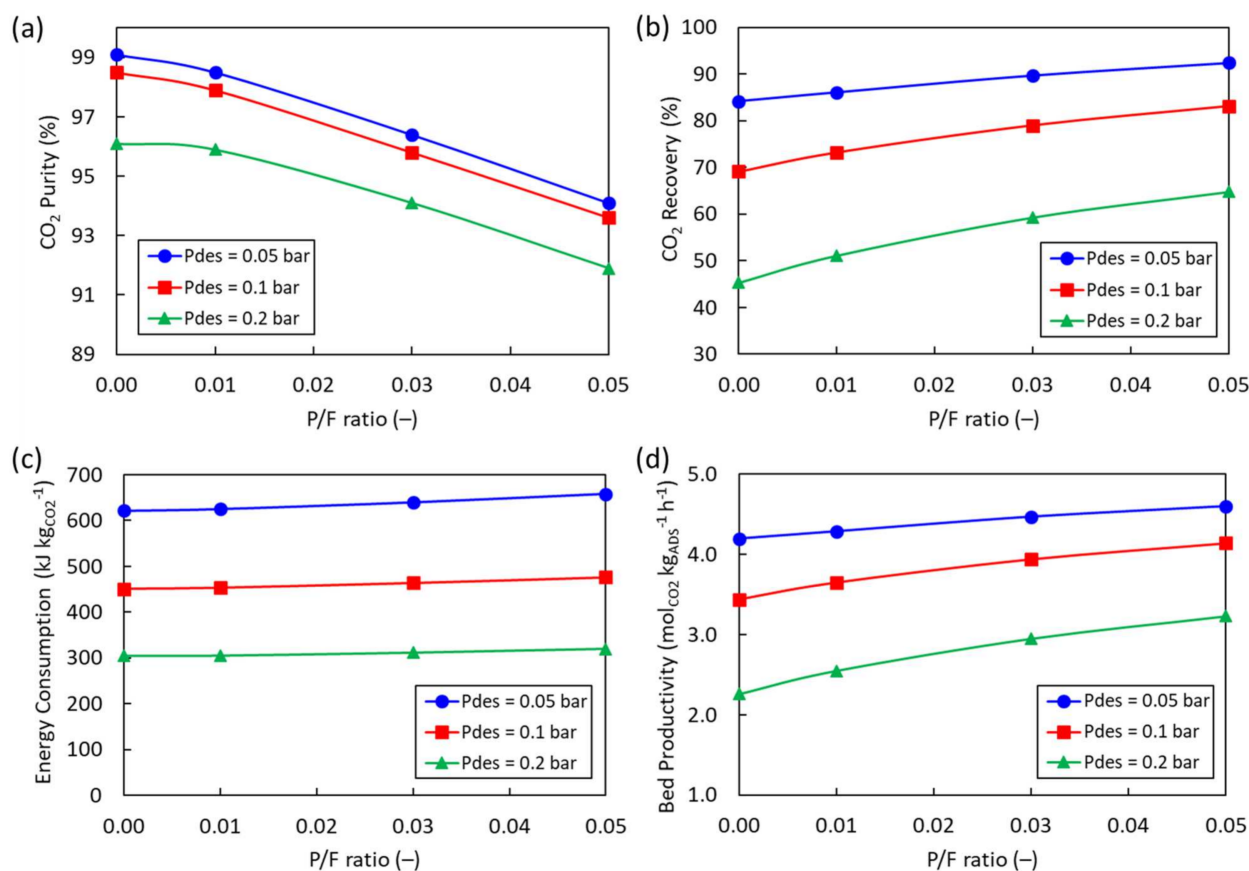


Figure 5. Evolution of the KPIs of the 2-bed, 6-step VPSA with the purge-to-feed ratio and desorption pressure: (a) CO₂ purity; (b) CO₂ recovery; (c) Specific energy consumption; (d) Bed productivity.

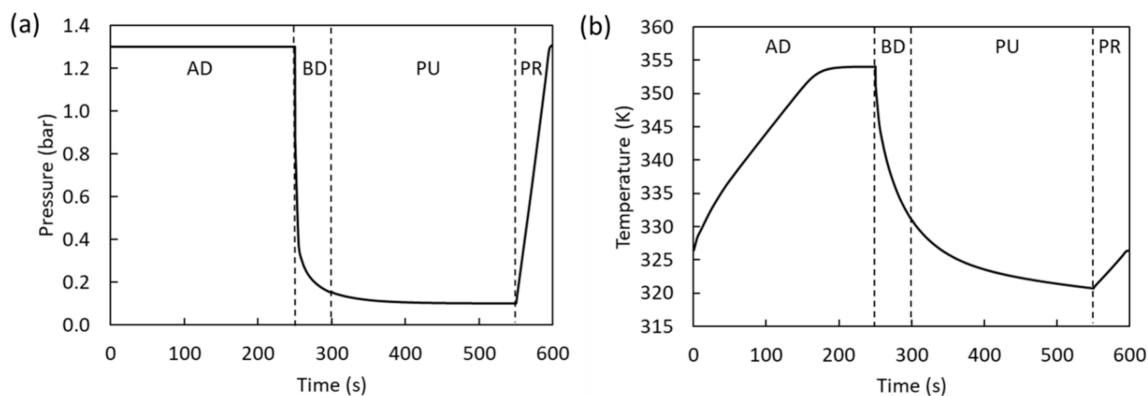


Figure 6. Profiles of (a) pressure and (b) temperature averaged over the bed length for a cycle at the cyclic steady state of the 2-bed, 4-step VPSA (Run 6).

Focusing on the best simulation runs in Tables 3 and 4, CO₂ purity and specific energy consumption against CO₂ recovery trade-offs are shown in Figure 8 where the P/F ratio varied while the desorption pressure was fixed at 0.05 bar. The superiority of the 2-bed, 6-step configuration over the 2-bed, 4-step configuration is clearly visible. With a fixed CO₂ recovery on the X-axis, the CO₂ purity is 4.1% higher on average while the specific energy consumption is 4.8% lower on average.

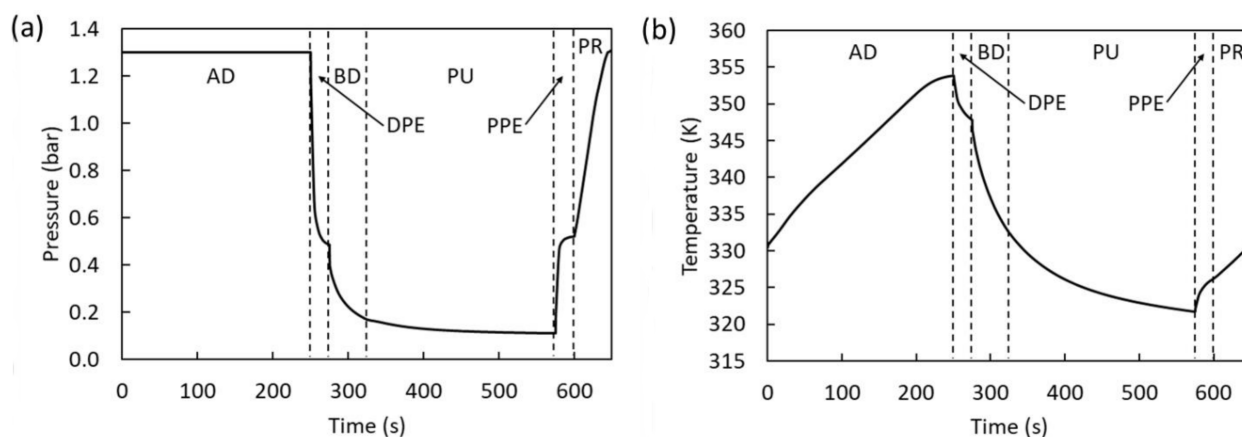


Figure 7. Profiles of (a) pressure and (b) temperature averaged over the bed length for a cycle at the cyclic steady state of the 2-bed, 6-step VPSA (Run 18).

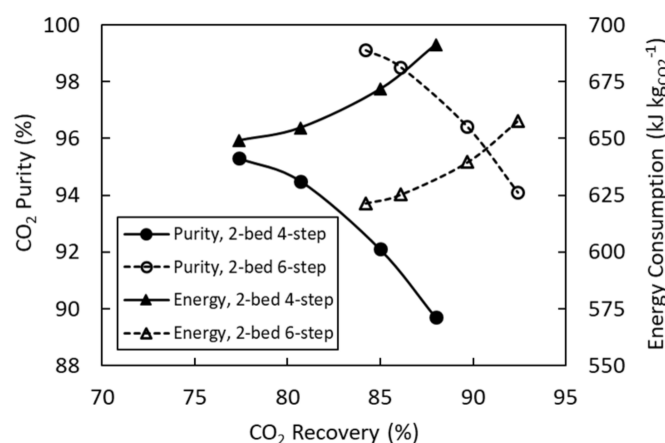


Figure 8. CO₂ purity and specific energy consumption against CO₂ recovery for the VPSA process with varying purge-to-feed ratio and desorption pressure at 0.05 bar.

This outcome is also confirmed by analysing the gas phase composition in the fixed beds at cyclic steady state. Figure 9 shows the profiles of CO₂ and the other component mole fractions with respect to the dimensionless axial distance along the bed (z/L_b) at the end of the adsorption step for both VPSA configurations. In particular, the figure shows Run 1 as the optimal simulation for the 2-bed, 4-step cycle configuration and Run 15 as the optimal simulation for the 2-bed, 6-step cycle configuration, both of which have a CO₂ purity greater than 95%. However, due to the pressure equalization step and the higher P/F ratio, Run 15 clearly exhibits sharper mass transfer zones (MTZ) than Run 1 so that the CO₂ concentration front progresses less towards the product end at the end of the adsorption step (Figure 9a). This results in less CO₂ being lost during the adsorption step, leading to a higher CO₂ recovery during the blowdown step and the purge step (89.7% against 77.4%).

As already mentioned, a few studies in the literature designed and simulated VPSA CO₂ capture processes applied to SMR-based hydrogen plant tail gas. Table 5 shows the performance comparison between such works and the VPSA systems designed in this study. For a fair comparison, all specific energy consumptions were evaluated considering 100% efficiency for the vacuum pump. The operating conditions reported in Golmakani et al. [22] are quite similar to those of the current study. Therefore, the lower CO₂ purities and recoveries can be mainly explained by the poorer CO₂ adsorption capacities and selectivities of the selected adsorbents, namely SAPO-34 zeolite, activated carbon and 5A zeolite, compared to NaX zeolite. The simulation runs reported by Shi et al. [23] achieved either a CO₂ purity or a CO₂ recovery greater than 95% and 90%, respectively, using

silica gel and fixing the desorption pressure at 0.2 bar. Accordingly, the specific energy consumption was around half of the current study. The separation performance could be further improved by reducing the desorption pressure, but it should be noted that the authors considered a PSA tail gas feed with a CO mole fraction of only 1.5%, which is substantially lower than 14.7% used in this study. This large difference in impurity content in the feed would heavily affect the separation performance. In conclusion, the NaX zeolite-based 2-bed, 6-step configuration proposed in this study is so far one of the most promising VPSA processes able to achieve 95+% CO₂ purity and 90+% CO₂ recovery simultaneously, therefore serving as an efficient technology to decarbonize existing hydrogen plants and produce blue H₂.

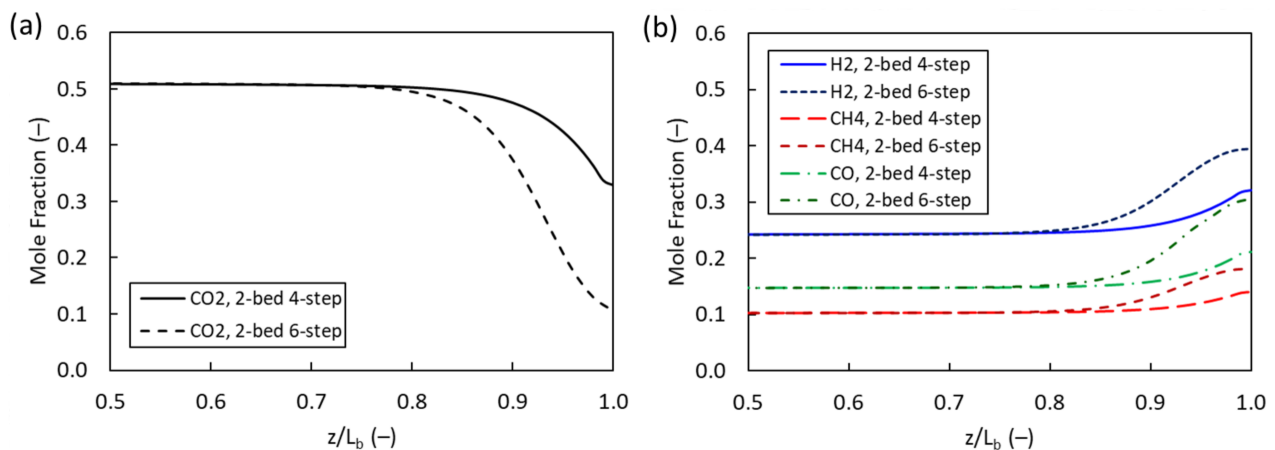


Figure 9. Profiles of (a) CO₂ mole fraction and (b) other component mole fractions along the dimensionless axial bed distance at the end of the adsorption step for the 2-bed, 4-step VPSA (Run 1) and the 2-bed, 6-step VPSA (Run 15).

Table 5. Performance comparison of CO₂ capture processes applied to SMR-based hydrogen plant tail gas using VPSA technology.

Cycle Configuration	Adsorbent	P_{ads} (bar)	P_{des} (bar)	P/F Ratio (-)	CO ₂ Purity (%)	CO ₂ Recovery (%)	Specific Energy Consumption (kJ kgCO ₂ ⁻¹) ¹	Bed Productivity (molCO ₂ h ⁻¹ kg _{ads} ⁻¹)	Reference
2-bed, 4-step 2-bed, 6-step	NaX zeolite	1.3	0.05	0	95.3	77.4	259.6	5.57	This study
				0.03	96.4	89.7	255.9	4.47	
4-bed, 7-step	SAPO-34 zeolite	4.0	0.05	0.03	90.5	73.5	305.0	3.34	[22]
	Activated carbon				86.2	56.8	369.0	3.14	
	5A zeolite				88.1	75.9	284.0	3.61	
3-bed, 5-step	Silica gel	2.0	0.2	N/A	97.1 88.6	82.6 97.8	133.3 133.6	N/A	[23]

¹ All values were evaluated considering 100% efficiency for the vacuum pump.

5. Conclusions

In this work, we designed and numerically investigated for the first time a VPSA process capable of capturing CO₂ from the PSA tail gas of an industrial SMR-based hydrogen plant equipped with a conventional single stage high temperature WGS reactor. The PSA tail gas, having a CO₂ concentration of 50+ mol%, is expected to be the most economically efficient carbon capture location to retrofit existing hydrogen plants via VPSA technology, thus allowing the production of blue H₂. The VPSA systems were rigorously simulated by a mathematical model integrating mass, momentum and energy balances. The separation on NaX zeolite was assessed using the IAS theory coupled with the dual-site Langmuir model as well as a temperature-dependent LDF model.

Two different cycle configurations were investigated, namely a 2-bed, 4-step Skarstrom cycle and 2-bed, 6-step modified Skarstrom cycle with pressure equalization, as well as various operating conditions including the purge-to-feed ratio ranging 0–0.05 and the desorption pressure ranging 0.05–0.2 bar. We found that, with a desorption pressure of 0.05 bar, the 2-bed, 4-step configuration achieved 95.3% CO₂ purity and 77.4% CO₂ recovery while the 2-bed, 6-step configuration managed to reach 96.4% CO₂ purity and 89.7% CO₂ recovery. The bed productivity and the specific energy consumption of the latter configuration were 4.47 mol_{CO₂} h⁻¹ kg_{ads}⁻¹ and 639.7 kJ kg_{CO₂}⁻¹, respectively. The benefit of incorporating the pressure equalization step in the adsorption cycle was also confirmed by analyzing the gas phase composition in the adsorption beds at cyclic steady state. Compared to similar works reported in the literature, the 2-bed, 6-step VPSA process proposed in this study showed superior separation performances, therefore serving as an efficient technology to decarbonize existing hydrogen plants and produce blue H₂.

Future research will entail carrying out a rigorous economic analysis of the designed industrial VPSA unit to estimate CAPEX and OPEX other than the electric power consumption of the vacuum pumps. A techno-economic comparison with a VPSA unit designed to capture CO₂ from the flue gas of the SMR-based hydrogen plant [16] would also be pivotal to quantify the extra cost associated with an increased CO₂ capture rate.

Author Contributions: Conceptualization, M.L.; methodology, M.L.; software, M.L. and A.B.; investigation, M.L. and A.B.; writing—original draft preparation, M.L.; writing—review and editing, M.B. and M.C.; revised draft—review and editing, M.L., M.B. and M.C.; supervision, M.L. All authors have read and agreed to the published version of the manuscript.

Funding: This research received no external funding.

Institutional Review Board Statement: Not applicable.

Informed Consent Statement: Not applicable.

Data Availability Statement: Not applicable.

Conflicts of Interest: The authors declare no conflict of interest.

Nomenclature

A_b	Bed surface area (m ²)
$b_{1,i}$	Equilibrium constant of component <i>i</i> for site 1 (bar ⁻¹)
$b_{2,i}$	Equilibrium constant of component <i>i</i> for site 2 (bar ⁻¹)
$b_{1,i,0}$	Pre-exponential equilibrium constant coefficient of component <i>i</i> for site 1 (bar ⁻¹)
$b_{2,i,0}$	Pre-exponential equilibrium constant coefficient of component <i>i</i> for site 2 (bar ⁻¹)
c_i	Gas phase concentration of component <i>i</i> (mol m ⁻³)
$c_{p,s}$	Adsorbent particle specific heat capacity (J kg ⁻¹ K ⁻¹)
c_T	Total gas phase concentration (mol m ⁻³)
C_v	Valve flow coefficient (kg s ⁻¹ Pa ^{-1/2})
D_b	Bed diameter (m)
D_m	Molecular diffusivity (m ² s ⁻¹)
d_p	Adsorbent particle diameter (m)
D_z	Axial mass dispersion coefficient (m ² s ⁻¹)
F	Mass flowrate (kg s ⁻¹)
F_i	Assigned mass flowrate (kg s ⁻¹)
$(-\Delta H_{1,i})$	Heat of adsorption of component <i>i</i> for site 1 (J mol ⁻¹)
$(-\Delta H_{2,i})$	Heat of adsorption of component <i>i</i> for site 2 (J mol ⁻¹)
$(-\overline{\Delta H}_i)$	Averaged heat of adsorption of component <i>i</i> (J mol ⁻¹)
H_g	Gas phase enthalpy per unit volume (J m ⁻³)
h_w	Heat transfer coefficient between the gas phase and the bed wall (W m ⁻² K ⁻¹)
J_i	Diffusive flux of component <i>i</i> (mol m ⁻² s ⁻¹)
J_T	Thermal diffusive flux (W m ⁻²)

k_g	Gas thermal conductivity ($W m^{-1} K^{-1}$)
$k_{LDF,i}$	LDF coefficient of component i (s^{-1})
$k_{1,i}$	First parameter of LDF coefficient linear equation of component i ($s^{-1} K^{-1}$)
$k_{2,i}$	Second parameter of LDF coefficient linear equation of component i (s^{-1})
k_z	Axial thermal dispersion coefficient ($W m^{-1} K^{-1}$)
L_b	Bed length (m)
m_{ads}	Adsorbent mass (kg)
MW_i	Molecular weight of component i ($kg mol^{-1}$)
P	Pressure (bar)
ΔP	Pressure difference (bar)
P_{ads}	Adsorption pressure (bar)
P_{atm}	Atmospheric pressure (bar)
P_{des}	Desorption pressure (bar)
P_i	Partial pressure of component i (bar)
P_i^0	Surface pressure of component i (bar)
Pr	Prandtl number (-)
P/F	Purge-to-feed ratio (-)
q_i^*	Adsorbed phase concentration of component i at equilibrium ($mol kg^{-1}$)
\bar{q}_i	Averaged adsorbed phase concentration of component i ($mol kg^{-1}$)
$q_{s1,i}$	Saturation capacity of component i for site 1 ($mol kg^{-1}$)
$q_{s2,i}$	Saturation capacity of component i for site 2 ($mol kg^{-1}$)
q_T	Total adsorbed phase concentration ($mol kg^{-1}$)
R	Ideal gas constant ($J mol^{-1} K^{-1}$)
Re	Reynolds number (-)
Sc	Schmidt number (-)
t	Time (s)
t_{AD}	Adsorption time (s)
t_{BD}	Blowdown time (s)
t_{cycle}	Cycle time (s)
t_{DPE}	Depressurizing pressure equalization time (s)
t_{PPE}	Pressurizing pressure equalization time (s)
t_{PR}	Feed pressurization time (s)
t_{PU}	Purge time (s)
T	Temperature (K)
T_w	Bed wall temperature (K)
u	Interstitial gas velocity ($m s^{-1}$)
U_g	Gas phase internal energy per unit volume ($J m^{-3}$)
U_s	Adsorbent particle internal energy per unit volume ($J m^{-3}$)
V_{SP}	Valve stem position (-)
x_i	Adsorbed phase molar fraction of component i (-)
y_i	Gas phase molar fraction of component i (-)
z	Axial distance along the bed (m)
Greek letters	
γ	Ratio of specific heat capacities c_p/c_v (-)
ε	External bed void fraction (-)
ε_p	Adsorbent particle void fraction (-)
η	Vacuum pump efficiency (-)
μ	Gas viscosity (Pa s)
ρ_g	Gas density ($kg m^{-3}$)
ρ_s	Adsorbent particle density ($kg m^{-3}$)
ψ_{eq}	Reduced grand potential at equilibrium ($mol kg^{-1}$)
ψ_i	Reduced grand potential of component i ($mol kg^{-1}$)

References

1. IEA. Global Energy Review: CO₂ Emissions in 2020. 2021. Available online: <https://www.iea.org/articles/global-energy-review-co2-emissions-in-2020> (accessed on 28 December 2021).
2. IEA. The Future of Hydrogen. 2019. Available online: <https://www.iea.org/reports/the-future-of-hydrogen> (accessed on 28 December 2021).

3. BEIS. UK Hydrogen Strategy. 2021. Available online: <https://www.gov.uk/government/publications/uk-hydrogen-strategy> (accessed on 28 December 2021).
4. Meyers, R.A. *Handbook of Petroleum Refining Processes*, 3rd ed.; McGraw-Hill: New York, NY, USA, 2004.
5. Collodi, G. Hydrogen production via steam reforming with CO₂ capture. *Chem. Eng. Trans.* **2010**, *19*, 37–42.
6. Meerman, J.C.; Hamborg, E.S.; van Keulen, T.; Ramirez, A.; Turkenburg, W.C.; Faaij, A.P.C. Techno-economic assessment of CO₂ capture at steam methane reforming facilities using commercially available technology. *Int. J. Greenh. Gas Control* **2012**, *9*, 160–171. [[CrossRef](#)]
7. Voss, C. CO₂ removal by PSA: An industrial view on opportunities and challenges. *Adsorption* **2014**, *20*, 295–299. [[CrossRef](#)]
8. IEA. The Shell Quest Carbon Capture and Storage Project. 2019. Available online: <https://ieaghg.org/publications/technical-reports/reports-list/9-technical-reports/949-2019-04-the-shell-quest-carbon-capture-and-storage-project> (accessed on 28 December 2021).
9. IEA. The Carbon Capture Project at Air Products' Port Arthur Hydrogen Production Facility. 2018. Available online: <https://ieaghg.org/publications/technical-reports/reports-list/9-technical-reports/956-2018-05-the-ccs-project-at-air-products-port-arthur-hydrogen-production-facility> (accessed on 28 December 2021).
10. IEA. Reference Data and Supporting Literature Review for SMR Based Hydrogen Production with CCS. 2017. Available online: <https://ieaghg.org/publications/technical-reports/reports-list/10-technical-reviews/778-2017-tr3-reference-data-supporting-literature-reviews-for-smr-based-hydrogen> (accessed on 28 December 2021).
11. Park, J.H.; Beum, H.T.; Kim, J.N.; Cho, S.H. Numerical analysis on the power consumption of the PSA process for recovering CO₂ from flue gas. *Ind. Eng. Chem. Res.* **2002**, *41*, 4122–4131. [[CrossRef](#)]
12. Xiao, P.; Zhang, J.; Webley, P.; Li, G.; Singh, R.; Todd, R. Capture of CO₂ from flue gas streams with zeolite 13X by vacuum-pressure swing adsorption. *Adsorption* **2008**, *14*, 575–582. [[CrossRef](#)]
13. Luberti, M.; Oreggioni, G.D.; Ahn, H. Design of a rapid vacuum pressure swing adsorption process for post-combustion CO₂ capture from a biomass-fuelled CHP plant. *J. Environ. Chem. Eng.* **2017**, *5*, 3973–3982. [[CrossRef](#)]
14. Ruthven, D.M.; Farooq, S.; Knaebel, K.S. *Pressure Swing Adsorption*; VCH Publishers: New York, NY, USA, 1994.
15. Figueroa, J.D.; Fout, T.; Plasynski, S.; McIlvried, H.; Srivastava, R.D. Advances in CO₂ capture technology—The U.S. Department of Energy's Carbon Sequestration Program. *Int. J. Greenh. Gas Control* **2008**, *2*, 9–20. [[CrossRef](#)]
16. Capocelli, M.; Luberti, M.; Inno, S.; D'Antonio, F.; Di Natale, F.; Lancia, A. Post-combustion CO₂ capture by RVPSA in a large-scale steam reforming plant. *J. CO₂ Util.* **2019**, *32*, 53–65. [[CrossRef](#)]
17. Oreggioni, G.D.; Brandani, S.; Luberti, M.; Baykan, Y.; Friedrich, D.; Ahn, H. CO₂ capture from syngas by an adsorption process at a biomass gasification CHP plant: Its comparison with amine-based CO₂ capture. *Int. J. Greenh. Gas Control* **2015**, *35*, 71–81. [[CrossRef](#)]
18. Liu, B.; Yu, X.; Shi, W.; Shen, Y.; Zhang, D.; Tang, Z. Two-stage VSA/PSA for capturing carbon dioxide (CO₂) and producing hydrogen (H₂) from steam methane reforming gas. *Int. J. Hydrogen Energy* **2020**, *45*, 24870–24882. [[CrossRef](#)]
19. Sircar, S.; Kratz, W.C. Simultaneous production of hydrogen and carbon dioxide from steam reformer off-gas by pressure swing adsorption. *Sep. Sci. Technol.* **1988**, *23*, 2397–2415. [[CrossRef](#)]
20. Streb, A.; Hefti, M.; Gazzani, M.; Mazzotti, M. Novel adsorption process for co-production of hydrogen and CO₂ from a multicomponent stream. *Ind. Eng. Chem. Res.* **2019**, *58*, 17489–17506. [[CrossRef](#)]
21. Streb, A.; Mazzotti, M. Novel adsorption process for co-production of hydrogen and CO₂ from a multicomponent stream—Part 2: Application to steam methane reforming and autothermal reforming gases. *Ind. Eng. Chem. Res.* **2020**, *59*, 10093–10109. [[CrossRef](#)]
22. Golmakani, A.; Fatemi, S.; Tamnanloo, J. CO₂ capture from the tail gas of hydrogen purification unit by vacuum swing adsorption process, using SAPO-34. *Ind. Eng. Chem. Res.* **2016**, *55*, 334–350. [[CrossRef](#)]
23. Shi, W.; Yang, H.; Shen, Y.; Fu, Q.; Zhang, D.; Fu, B. Two-stage PSA/VSA to produce H₂ with CO₂ capture via steam methane reforming (SMR). *Int. J. Hydrogen Energy* **2018**, *43*, 19057–19074. [[CrossRef](#)]
24. Mhaskar, P.R.; Moharir, A.S. Heuristics for synthesis and design of pressure-swing adsorption processes. *Adsorption* **2012**, *18*, 275–295. [[CrossRef](#)]
25. Brea, P.; Delgado, J.A.; Agueda, V.I.; Gutierrez, P.; Uguina, M.A. Multicomponent adsorption of H₂, CH₄, CO and CO₂ in zeolites NaX, CaX and MgX. Evaluation of performance in PSA cycles for hydrogen purification. *Microporous Mesoporous Mater.* **2019**, *286*, 187–198. [[CrossRef](#)]
26. Wang, L.; Liu, Z.; Li, P.; Wang, J.; Yu, J. CO₂ capture from flue gas by two successive VPSA units using 13XAPG. *Adsorption* **2012**, *18*, 445–459. [[CrossRef](#)]
27. Krishnamurthy, S.; Rao, V.R.; Guntuka, S.; Sharratt, P.; Haghpanah, R.; Rajendran, A.; Amanullah, M.; Karimi, I.A.; Farooq, S. CO₂ capture from dry flue gas by vacuum swing adsorption: A pilot plant study. *AIChE J.* **2014**, *60*, 1830–1842. [[CrossRef](#)]
28. Luberti, M.; Friedrich, D.; Brandani, S.; Ahn, H. Design of a H₂ PSA for cogeneration of ultrapure hydrogen and power at an advanced integrated gasification combined cycle with pre-combustion capture. *Adsorption* **2014**, *20*, 511–524. [[CrossRef](#)]
29. Luberti, M.; Ahn, H. Design of an industrial multi-bed (V)PSA unit for argon concentration. *Sep. Purif. Technol.* **2021**, *261*, 118254. [[CrossRef](#)]
30. Luberti, M.; Kim, Y.-H.; Lee, C.-H.; Ferrari, M.-C.; Ahn, H. New momentum and energy balance equations considering kinetic energy effect for mathematical modelling of a fixed bed adsorption column. *Adsorption* **2015**, *21*, 353–363. [[CrossRef](#)]
31. Ergun, S. Fluid flow through packed columns. *Chem. Eng. Prog.* **1952**, *48*, 89–94.

32. Myers, A.L.; Prausnitz, J.M. Thermodynamics of mixed-gas adsorption. *AIChE J.* **1965**, *11*, 121–127. [[CrossRef](#)]
33. Santori, G.; Luberti, M. Thermodynamics of thermally-driven adsorption compression. *Sustain. Mater. Technol.* **2016**, *10*, 1–9. [[CrossRef](#)]
34. OriginLab. 2019. Available online: <https://www.originlab.com/> (accessed on 28 December 2021).
35. Wakao, N.; Funazkri, T. Effect of fluid dispersion coefficients on particle-to-fluid mass transfer coefficients in packed beds. *Chem. Eng. Sci.* **1978**, *33*, 1375–1384. [[CrossRef](#)]
36. Specchia, V.; Baldi, G.; Sicardi, S. Heat transfer in packed bed reactors with one phase flow. *Chem. Eng. Commun.* **1980**, *4*, 361–380. [[CrossRef](#)]
37. Process System Enterprise Ltd. 2020. Available online: <https://www.psenterprise.com/> (accessed on 28 December 2021).
38. Liu, Z.; Grande, C.A.; Li, P.; Yu, J.; Rodrigues, A.E. Multi-bed vacuum pressure swing adsorption for carbon dioxide capture from flue gas. *Sep. Purif. Technol.* **2011**, *81*, 307–317. [[CrossRef](#)]
39. IEA. Techno-Economic Evaluation of SMR Based Standalone (Merchant) Hydrogen Plant with CSS. 2017. Available online: <https://ieaghg.org/component/content/article/49-publications/technical-reports/784-2017-02-smr-based-h2-plant-with-ccs> (accessed on 28 December 2021).
40. Yang, R.T. *Gas Separation by Adsorption Processes*; Butterworths: Boston, MA, USA, 1987.